

# Relaxin receptor deficiency promotes vascular inflammation and impairs outward remodeling in arteriovenous fistulas

Taisiya Bezhaeva,<sup>\*,†</sup> Margreet R. de Vries,<sup>†,‡</sup> Wouter J. Geelhoed,<sup>\*,†</sup> Eric P. van der Veer,<sup>\*,†</sup> Sabine Versteeg,<sup>§,¶,||</sup> Carla M. A. van Alem,<sup>\*,†</sup> Bram M. Voorzaat,<sup>\*</sup> Niels Eijkelkamp,<sup>§,¶,||</sup> Koen E. van der Bogt,<sup>\*,#</sup> Alexander I. Agoulnik,<sup>\*\*</sup> Anton-Jan van Zonneveld,<sup>\*,†</sup> Paul H. A. Quax,<sup>†,‡</sup> and Joris I. Rotmans<sup>\*,†,1</sup>

<sup>\*</sup>Department of Internal Medicine, <sup>†</sup>Eindhoven Laboratory for Vascular and Regenerative Medicine, and <sup>‡</sup>Department of Surgery, Leiden University Medical Center, Leiden, The Netherlands; <sup>§</sup>Laboratory of Translational Immunology, <sup>¶</sup>Laboratory of Neuroimmunology, and <sup>||</sup>Laboratory of Developmental Origins of Disease, University Medical Center Utrecht, Utrecht, The Netherlands; <sup>#</sup>Department of Surgery, Haaglanden Medical Center, The Hague, The Netherlands; and <sup>\*\*</sup>Department of Human and Molecular Genetics, Herbert Wertheim College of Medicine, Florida International University, Miami, Florida, USA

**ABSTRACT:** The pathophysiology of arteriovenous fistula (AVF) maturation failure is not completely understood but impaired outward remodeling (OR) and intimal hyperplasia are thought to be contributors. This adverse vascular response after AVF surgery results from interplay between vascular smooth muscle cells (VSMCs), the extracellular matrix (ECM), and inflammatory cells. Relaxin (RLN) is a hormone that acts on the vasculature *via* interaction with RLN/insulin-like peptide family receptor 1 (RXFP1), resulting in vasodilatation, ECM remodeling, and decreased inflammation. In the present study, we evaluated the consequences of RXFP1 knockout (*Rxfp1*<sup>-/-</sup>) on AVF maturation in a murine model of AVF failure. *Rxfp1*<sup>-/-</sup> mice showed a 22% decrease in vessel size at the venous outflow tract 14 d after AVF surgery. Furthermore, a 43% increase in elastin content was observed in the lesions of *Rxfp1*<sup>-/-</sup> mice and coincided with a 41% reduction in elastase activity. In addition, *Rxfp1*<sup>-/-</sup> mice displayed a 6-fold increase in CD45<sup>+</sup> leukocytes, along with a 2-fold increase in monocyte chemoattractant protein 1 (MCP1) levels, when compared with wild-type mice. *In vitro*, VSMCs from *Rxfp1*<sup>-/-</sup> mice exhibited a synthetic phenotype, as illustrated by augmentation of collagen, fibronectin, TGF- $\beta$ , and platelet-derived growth factor mRNA. In addition, VSMCs derived from *Rxfp1*<sup>-/-</sup> mice showed a 5-fold increase in cell migration. Finally, RXFP1 and RLN expression levels were increased in human AVFs when compared with unoperated cephalic veins. In conclusion, RXFP1 deficiency hampers elastin degradation and results in induced vascular inflammation after AVF surgery. These processes impair OR in murine AVF, suggesting that the RLN axis could be a potential therapeutic target for promoting AVF maturation.—Bezhaeva, T., de Vries, M. R., Geelhoed, W. J., van der Veer, E. P., Versteeg, S., van Alem, C. M. A., Voorzaat, B. M., Eijkelkamp, N., van der Bogt, K. E., Agoulnik, A. I., van Zonneveld, A.-J., Quax, P. H. A., Rotmans, J. I. Relaxin receptor deficiency promotes vascular inflammation and impairs outward remodeling in arteriovenous fistulas. *FASEB J.* 32, 6293–6304 (2018). www.fasebj.org

**KEY WORDS:** hemodialysis vascular access • RXFP1 • macrophages • VSMC • extracellular matrix

**ABBREVIATIONS:**  $\alpha$ SMA, SM- $\alpha$ -actin; AVF, arteriovenous fistula; CCR2, chemokine receptor type 2; DAB, 3,3'-diaminobenzidine; ECM, extracellular matrix; FBS, fetal bovine serum; GR1, granulocytic marker; HEPES, 4-(2-hydroxyethyl)-1-piperazineethanesulfonic acid; IEL, internal elastic lamina; IH, intimal hyperplasia; MAC3, macrophage marker; MCP1, monocyte chemoattractant protein 1; NHS, normal human serum; OR, outward remodeling; RLN, relaxin; RXFP1, relaxin/insulin-like peptide family receptor 1; VSMC, vascular smooth muscle cell; WT, wild type

<sup>1</sup> Correspondence: Department of Internal Medicine, C7Q-36, Leiden University Medical Center, Albinusdreef 2, 2333ZA Leiden, The Netherlands. E-mail: j.i.rotmans@lumc.nl

doi: 10.1096/fj.201800437R

This article includes supplemental data. Please visit <http://www.fasebj.org> to obtain this information.

A properly functioning vascular access site is a crucial lifeline for patients required to undergo hemodialysis. Although an arteriovenous fistula (AVF) remains the vascular access of choice, the frequency of primary AVF failure is ~40% (1). Moreover, the primary patency rates 1 yr after creation do not exceed 60% (2), making vascular access-related complications one of the most common causes of hospitalization and morbidity in hemodialysis patients.

Although the pathophysiology of AVF maturation failure is incompletely understood, it is well established that both intimal hyperplasia (IH) and outward remodeling

(OR) of the arteriovenous conduit ultimately determine luminal dimensions, fistula flow and patency (3). Several studies have shown that vascular adaptation of the arteriovenous conduit is characterized by an inflammatory response that coincides with flow-mediated remodeling of the extracellular matrix (ECM) and proliferation and migration of vascular smooth muscle cells (VSMCs) (4–11).

Relaxin (RLN) is a 6-kDa peptide hormone, originally known for its role in the growth and differentiation of the reproductive tract, and systemic hemodynamic adaptations during pregnancy, in particular vasodilatation (12–15). Three RLN genes, namely *RLN1*, 2, and 3, exist in humans, whereas rats and mice have 2 (*Rln1* and 3), with *Rln1* in rats and mice corresponding to human *RLN2* and representing the primary source of circulating RLN (16). In the last 20 yr, RLN has emerged as a pleiotropic hormone that serves critical functions irrespective of gender. The systemic effects mediated by *RLN2* on arterial mechanical properties include increasing arterial compliance, reducing systemic vascular resistance, and myogenic reactivity as demonstrated in rats and mice (12, 17–20). Furthermore, administration of recombinant *RLN2* ameliorates renal and cardiac fibrosis, stimulates ECM turnover, and moderates inflammation by reducing inflammatory cytokines (21–27).

In the context of AVF maturation, it is important to emphasize that *RLN2* is expressed in the vessel wall (28, 29) and that the observed vascular effects of *RLN2* are mediated through an interaction with *RLN*/insulin-like peptide family receptor 1 (RXFP1), a G-protein-coupled receptor. RXFP1 is primarily expressed on VSMCs and to a lesser extent on the cell surface of macrophages and endothelial cells of arteries and veins (30–32).

In light of the emerging role of the *RLN2*-RXFP1 axis in vascular remodeling and inflammation, we examined the consequences of disturbing this hormone–receptor balance in AVF maturation. For this purpose, we used a well-established murine AVF model to study the effect of RXFP1 deficiency on fistula remodeling. Furthermore, we determined the effects of RXFP1 deficiency on the phenotype and function of VSMCs *in vitro*.

## MATERIALS AND METHODS

### Animals

This study was performed in agreement with Dutch government guidelines and Directive 2010/63/EU of the European Parliament. All animal experiments were approved by the Institutional Committee for Animal Welfare of both Leiden University Medical Center and University Medical Center Utrecht. The phenotype of *Rxfp1*<sup>-/-</sup> mice has been previously described (33). Male wild-type (WT, C57BL/6, *n* = 10) and *Rxfp1*<sup>-/-</sup> mice (C57BL/6, *n* = 10), were bred in the animal facility at the University Medical Center Utrecht. All animals were given water and chow *ad libitum*. Adult male mice aged 10–13 wk were used for the experiments. AVFs were created in an end-to-side manner between the dorsomedial branch of the external jugular vein and the common carotid artery as previously described (5, 34). Briefly, the animal was anesthetized using isoflurane before the skin of the ventral neck area was shaved and disinfected. The mouse was then fixed in a supine position on a heating blanket and injected with

buprenorphin (0.1 mg/kg; MSD, Kenilworth, NJ, USA) and 0.5 ml saline. Under a dissecting microscope (Leica, Wetzlar, Germany), an incision in the ventral midline of the neck area was made, followed by a dissection of the right dorsomedial branch of the external jugular vein and ipsilateral common carotid artery after the excision of the sternocleidomastoid muscle using a heat cauterizer. Next, after applying a vascular clamp (S&T, Neuhausen, Switzerland) on the proximal and distal artery, an incision (~1 mm) was made using micro-scissors (Fine Science Tools, North Vancouver, BC, Canada) and the lumen was rinsed with heparin solution (100 IU/ml; LEO Pharma, Madison, NJ, USA). The vein was then clamped proximally, ligated distally, and transected just proximal to the ligation. After rinsing the vein with heparin solution, an end-to-side anastomosis was created using 10-0 interrupted sutures (B. Braun, Bethlehem, PA, USA). After completion of the anastomosis, the remaining clamps were removed and patency was assessed. The neck incision was closed with a 6-0 running suture (B. Braun). Following completion of the surgery, 0.5 ml of saline was injected subcutaneously and the mice were kept warm until recovery. The animals were euthanized 14 d after the surgical procedure.

### Blood pressure

Systolic blood pressure was assessed with the noninvasive tail cuff system in conscious mice before the AVF surgery and on d 7 and 14 after an AVF was created using the CODA system (Kent Scientific, Torrington, CT, USA). Animals were acclimated to the restrainer before measurements. Following the acclimation period, telemetry blood pressure measurements were acquired. Data segments (10 s each) were collected throughout each non-invasive measurement session (10 acclimation cycles followed by 20 measurement cycles).

### Arterial compliance

Aortas from *Rxfp1*<sup>-/-</sup> (*n* = 3) and WT (*n* = 5) mice were cannulated from the distal side at the base of the heart proximal to the abdominal area (1 cm in length) and placed immediately in ice-cold 4-(2-hydroxyethyl)-1-piperazineethanesulfonic acid (HEPES)-buffered physiologic saline solution. The vessels were subsequently placed in an *ex vivo* vessel perfusion system containing 37°C 10<sup>-4</sup> M papaverine in calcium-free HEPES-buffered physiologic saline solution. The vessel segments were tensioned to a longitudinal strain of 30 g and left to acclimatize for 15 min. The vessel segment was then exposed to a pressurized, cyclic flow at a rate of 60 ± 5 BPM, and the systolic pressure was gradually increased to 120 mmHg. Papaverine (10<sup>-4</sup> M) in calcium-free HEPES-buffered PBS was used as perfusate. The systolic and diastolic pressures throughout the test were recorded using a pressure sensor (700G Precision Pressure Test Gauge; Fluke, Everett, WA, USA). To measure vessel diameter, a microscope camera (Digital Microscope DSCO-P03; Cider House ICT, Endeavour Hills, VIC, Australia) capable of measuring with an accuracy of ±0.02 mm was placed above the perfused vessels. Recordings of each test were calibrated to the pressure and saved. To calculate arterial compliance, vessel diameter was measured during both the systolic and the diastolic phase of each pressure cycle. The dynamic compliance is provided as percentage compliance per 100 mmHg.

### Tissue harvesting and processing

The animals were anesthetized using isoflurane 14 d after AVF surgery. The venous and arterial limb of the AVF was dissected and a thoracotomy was performed whereupon the inferior vena

cava was transected followed by a fixation with 4% formalin through an intracardiac perfusion. The tissue was embedded in paraffin and 5  $\mu\text{m}$  sections of the venous outflow tract were cut perpendicular to the vein at intervals of 150  $\mu\text{m}$ .

### Morphometric and histologic analysis

All immunohistochemical and histochemical staining and measurements were performed on the first 3 venous cross-sections

downstream from the anastomosis. Weigert's elastin stain was used for the morphometric measurements. The area of the internal elastic lamina (IEL) was measured to assess the degree of OR (Fig. 1A). IH was calculated by subtracting the luminal area from the area within the IEL. Composition of the AVF lesions was further evaluated by staining for total leukocytes (CD45, 1:200; 550539; BD Biosciences, Franklin Lakes, NJ, USA) and macrophages [macrophage marker (MAC3), 1:200, 550292; BD Biosciences] in combination with CCR2 (chemokine receptor type 2) for a proinflammatory phenotype (1:400; ab32144; Abcam,

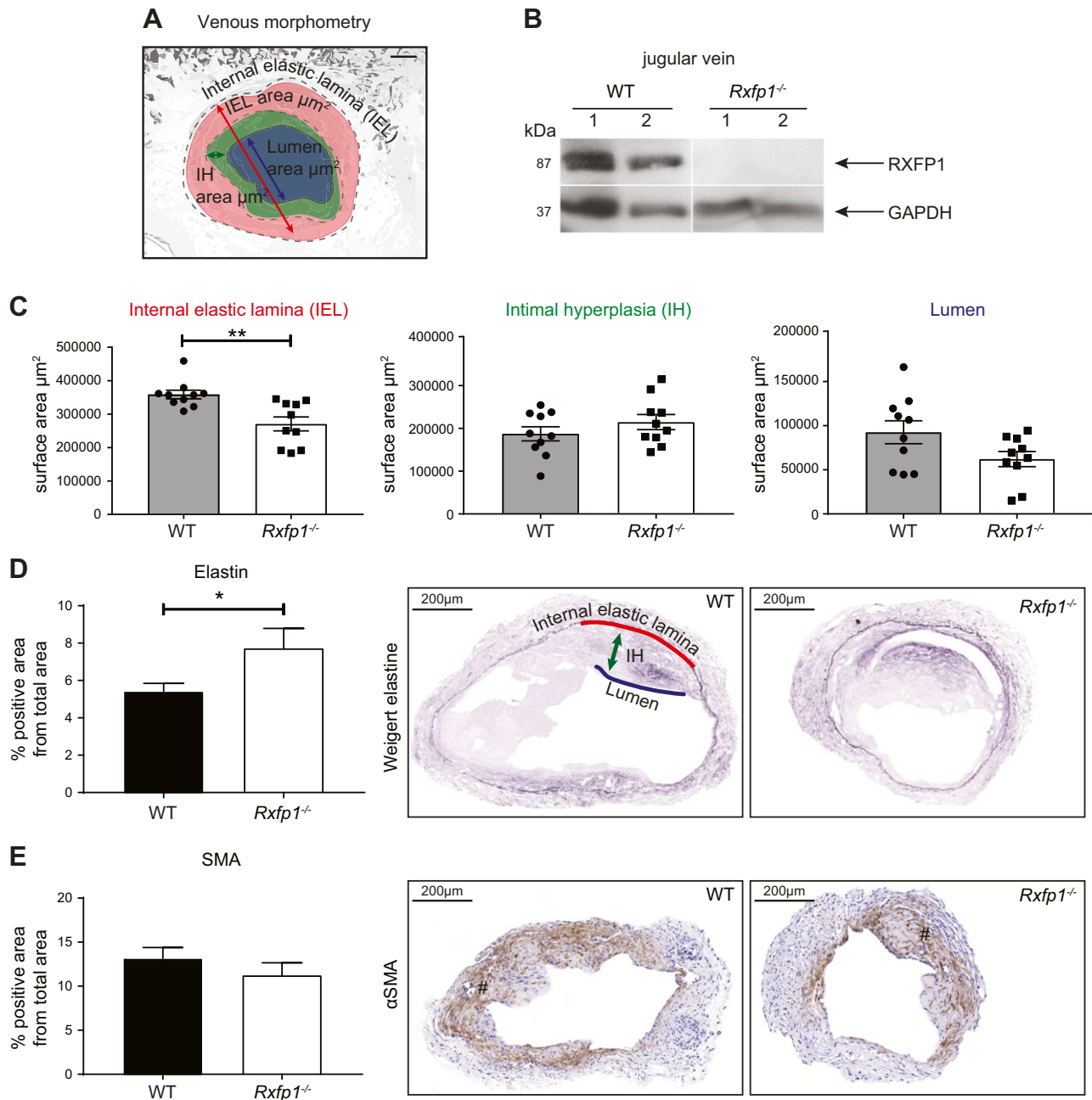


**Figure 1.** Morphometry and histology of the venous outflow tract of the AVF in *Rxfp1*<sup>-/-</sup> and WT mice 14 d after surgery. **A**) The area within the IEL (red) reflects the degree of OR of the venous outflow tract. IH (green) was calculated by subtracting the luminal area (blue) from the area within the IEL. **B**) Western blot of the jugular vein confirms the absence of RXFP1 protein in RXFP1-deficient mice. GAPDH was used as a loading control. **C**) Quantification of histomorphometry. RXFP1-deficient mice displayed decrease in the area of IEL (22%,  $P = 0.002$ ) and lumen (31%,  $P = 0.14$ ), whereas IH was comparable to that of WT mice. **D**) Increase in elastin deposition in the AVF lesions from *Rxfp1*<sup>-/-</sup> mice. **E**)  $\alpha$ SMA staining shows area of IH which did not differ between the groups. Weigert elastine staining was used to determine histomorphometrical parameters of the vessel. \* $P < 0.05$ ; \*\* $P < 0.005$  ( $n = 10/\text{group}$ ).

Cambridge, United Kingdom) or CD206 (1:1000, ab64693; Abcam) for an anti-inflammatory phenotype, neutrophils [granulocytic marker (GR1), 1:300; from G. Kraal, VU University Medical Center, Amsterdam, The Netherlands], T-lymphocytes (CD3, 1:300, ab32144; Abcam), and monocyte chemoattractant protein 1 (MCP1, 1:300, sc-1784; Santa Cruz Biotechnology, Dallas, TX, USA). VSMCs [SM- $\alpha$ -actin ( $\alpha$ SMA), 1:1000, M0851; Agilent Technologies, Santa Clara, CA, USA] were stained in a combination with Ki67 (1:200, 550609; BD Biosciences) to detect proliferating VSMCs.

All slides were digitized using an automated slide scanner (Pannoramic MIDI; 3DHistech, Budapest, Hungary). For the immunohistochemical analysis of the MAC3/CD206, MAC3/CCR2, and  $\alpha$ SMA/Ki67 staining, the number of positive cells was counted in 3 random fields of view at  $\times 400$  magnification, from which the mean was calculated. Quantification of CD45<sup>+</sup>, GR1<sup>+</sup>, CD3<sup>+</sup>, and MCP1 staining was performed with ImageJ software (National Institutes of Health, Bethesda, MD, USA) by calculating percentage of 3,3'-diaminobenzidine (DAB) positive area from the total vessel area.

### Cell culture

Primary arterial and venous VSMCs were isolated from the carotid artery and vena cava of C57BL/6 and *Rxfp1*<sup>-/-</sup> mice ( $n = 4$ /group), respectively. Connective tissues were removed and vessels cut open. The endothelial monolayer was detached by gently scraping with sterile surgical forceps. The carotid artery and caval vein were dissected into small pieces and plated onto fibronectin-coated Petri dishes (0.1 mg/ml) 100 or 60 mm in diameter. After a 14 d culture in DMEM supplemented with 20% fetal bovine serum, 2 mM L-glutamine, 100 U/ml penicillin, and 100  $\mu$ g/ml streptomycin, cells were trypsinized and replated onto 6- or 12-well plates and cultured for 7 d. At 80–90% confluence, VSMCs were trypsinized and seeded at the required density for further functional assays.

### Western blot

Proteins from tissue lysates were harvested in RIPA buffer and subjected to SDS-PAGE. A bicinchronic acid assay was performed to ensure equal protein loads in each sample. RXFP1 was detected using primary antibodies (1:500, AP23446SU-S; OriGene Technologies, Rockville, MD, USA). Glyceraldehyde 3-phosphate dehydrogenase (GAPDH; 1:5000, 5174S, Cell Signaling Technology, Danvers, MA, USA) was used as a loading control. All tests used Bio-Rad TGX precast gels and were blotted on nitrocellulose 0.2  $\mu$ m using the Bio-Rad TurboBlot system (Hercules, CA, USA).

### RNA isolation, cDNA synthesis and quantitative RT-PCR

Total RNA was extracted from VSMCs using Trizol reagent (Thermo Fisher Scientific) according to the manufacturer's protocol. RNA was reverse transcribed using the M-MLV First-Strand Synthesis System (Thermo Fisher Scientific) and used for quantitative analysis of mouse genes (Supplemental Table 1) with SYBR Green Master Mix (Thermo Fisher Scientific). Murine  $\beta$ -actin was used as the standard housekeeping gene. The relative mRNA expression levels were determined using 2<sup>- $\Delta\Delta$ Ct</sup> method.

### VSMC migration and haptotaxis assays

Primary arterial and venous VSMCs from control and *Rxfp1*<sup>-/-</sup> mice were grown to confluence and made quiescent in cultured

medium supplemented with 1% FBS for 24 h. Cells were detached from the surface and suspended at a concentration of 100,000 cells/ml in culture medium supplemented with 1% FBS. Migration was assayed with inserts having 8  $\mu$ m pores in 24-well chemotaxis chambers using the CytoSelect Cell Migration Assay Kit (Cell Biolabs, San Diego, CA, USA). Haptotaxis was assayed by plating cells into Transwell inserts with collagen I-coated inserts (CytoSelect Cell Haptotaxis Assay; Cell Biolabs). After 16 h, migratory VSMCs were lysed and labeled with fluorescent dye according to the manufacturer's instructions. A gradient of 20% FBS was used. Quantification was performed by reading fluorescence at 480/520 nm.

### VSMC proliferation assay

Murine VSMCs, explanted from aortas and veins of control or *Rxfp1*<sup>-/-</sup> mice, were cultured as described in the previous section, divided into aliquots, and plated on a 96-well plate. Cells were quantified 24 h later using the CyQuant Direct Cell Proliferation Assay according to the manufacturer's instructions (Thermo Fisher Scientific).

### Elastase activity assay

Elastase activity was measured on total tissue lysates isolated from *Rxfp1*<sup>-/-</sup> and WT mice ( $n = 10$  per group) using the Enz-Chek Assay Kit (Thermo Fisher Scientific) according to the manufacturer's instructions. Briefly, 10  $\mu$ m sections of AVF were lysed in RIPA buffer and a bicinchronic acid assay was performed to ensure equal loading of protein in each sample. DQ elastin, a soluble bovine neck ligament elastin labeled with BODIPY FL dye (Thermo Fisher Scientific), was used as a substrate to quench the conjugate's fluorescence. In the presence of elastase, the nonfluorescent substrate is digested, yielding highly fluorescent fragments, which were measured with a microplate reader at an excitation wavelength of 480  $\pm$  20 nm and an emission wavelength of 528  $\pm$  20 nm.

### Collagen assay

Collagen content was analyzed using the QuickZyme Total Collagen Assay Kit (QuickZyme Biosciences, Leiden, The Netherlands) on samples of formaldehyde-fixed, paraffin-embedded venous tissues isolated from *Rxfp1*<sup>-/-</sup> and WT mice ( $n = 10$  per group). In brief, 5–10 tissue sections (10  $\mu$ m long) were hydrolyzed by overnight incubation at 95°C in a heat block. Upon hydrolysis, without any pretreatment, 35  $\mu$ l was used for collagen quantification using the QuickZyme Total Collagen Assay Kit (assay time 90 min). The assay measured the total amount of hydroxyproline, a representative for all collagen types, present in the sample. The assay results in a chromogen with a maximum absorbance of 570 nm.

### Human tissue specimens

Human cephalic veins before AVF surgery ( $n = 3$ ) and during surgical revisions of AVF ( $n = 3$ ) were obtained at the Leiden University Medical Center in accordance with guidelines set out by the Code for Proper Secondary Use of Human Tissue enforced by the Dutch Federation of Biomedical Scientific Societies, which conform to the principles outlined in the Declaration of Helsinki. Specimens were fixed with formalin, embedded in paraffin, and sectioned. The human AVF sections were stained with  $\alpha$ SMA (1:1000; M0851; Agilent Technologies), RLX2 (RLN2, 1:1000, ab183505; Abcam), and RXFP1 (1:4000, AP23446SU-S; OriGene Technologies).

For RXFP1 antibody validation, 3 human fistula samples were incubated with the primary antibody or isotype control, both at 1:4000 dilution. Human endometrium was used as a positive control. Briefly, after deparaffinization step endogenous peroxidase was suppressed by incubation in 1% H<sub>2</sub>O<sub>2</sub> for 15 min at room temperature. Sections were then blocked with 5% PBSA (NaPO<sub>4</sub>, NaCl, NaAz and 1% bovine serum albumin) and 5% normal human serum (NHS) for 30 min. Next, sections were incubated overnight at room temperature with the primary antibody or isotype control, diluted at 1:4000, in 1% PBS buffer without calcium and magnesium, supplemented with 5% NHS. After rinsing in PBS for 3 cycles of 5 min each, sections were incubated with rabbit Evison (Agilent) and 5% NHS for 30 min at room temperature. Specific signals were detected using DAB (MilliporeSigma, Burlington, MA, USA) as chromogen. The reaction was halted by rapidly rinsing the sections in tap water before subjecting tissue samples to conventional hemalaun counterstaining.

For immunofluorescent staining of double-positive  $\alpha$ SMA<sup>+</sup> and RXFP1<sup>+</sup> cells, after exposure to primary antibodies, tissue sections were counterstained with Alexa 568-conjugated goat antimouse IgG2a (1:250; A21134; Molecular Probes, Eugene, OR, USA) for  $\alpha$ SMA, and Alexa 488-conjugated secondary goat antirabbit IgG (1:250; A11008; Molecular Probes) for RXFP1. Secondary antibodies were diluted in 1% PBSA; 5% NHS was added to prevent nonspecific binding. Nuclei were visualized with ProLong Gold Antifade Mountant with DAPI (P369; Thermo Fisher Scientific) (Supplemental Fig. 6).

### Statistical analysis

Results are expressed as means  $\pm$  SEM and values of  $P < 0.05$  were considered statistically significant. Student's *t* tests and the Mann-Whitney *U* tests for parametric and nonparametric data, respectively, were used as appropriate. For all *in vitro* experiments, 4 samples from different animals were used (biological  $n = 4$ ). Every experiment within each animal was performed in triplicates (experimental triplicate  $n = 3$ ).

## RESULTS

### Surgical outcome and patency

In total, AVF surgery was successfully performed on 23 mice (WT:  $n = 12$ ;  $Rxfp1^{-/-}$ :  $n = 11$ ), of which 2 (17%) from the WT group and 1 (9%) from the  $Rxfp1^{-/-}$  group were occluded 14 d after surgery. The occluded AVFs were excluded from morphometric analysis, yielding 10 animals/group. The body weight of the mice was similar in both groups ( $29 \pm 3$  g) and remained stable until the end of experiment.

### Effect of RXFP1 deficiency on AVF maturation

To study the effect of RXFP1 deficiency on AVF maturation, we created AVFs in WT and  $Rxfp1^{-/-}$  mice in an end-to-side fashion between the jugular vein and carotid artery as previously described (34). Given that most of the stenotic lesions in human AVFs occur in the venous outflow tract, we harvested the first 3 consecutive venous sections downstream of the anastomotic area for morphometric analysis. The impact of RXFP1 deficiency on vessel morphology was evaluated by assessing both intimal and

luminal area as well as the area within the IEL, reflecting the degree of OR of the venous outflow tract (Fig. 1A). The absence of the RXFP1 protein in  $Rxfp1^{-/-}$  mice was confirmed by using Western blot to analyze total tissue lysates isolated from jugular veins (Fig. 1B). Mice deficient in RXFP1 showed a 22% decrease of the IEL area at the venous outflow tract when compared with WT mice ( $P = 0.002$ ). The luminal area of the venous outflow tract in  $Rxfp1^{-/-}$  mice was 31% smaller when compared with control mice, although this difference was not significant ( $P = 0.14$ ). The intimal area did not differ between groups (Fig. 1C). Arterial blood pressure and compliance did not significantly differ between  $Rxfp1^{-/-}$  and WT mice (Supplemental Fig. 1).

In terms of ECM remodeling, we observed a 43% increase in elastin content in  $Rxfp1^{-/-}$  mice over that of WT mice ( $P = 0.04$ ) (Fig. 1D), whereas collagen production was similar in both groups (Supplemental Fig. 2). In both WT and  $Rxfp1^{-/-}$  mice, the majority of intimal cells expressed  $\alpha$ SMA, indicating that these cells are primarily of VSMC or fibroblastic origin (Fig. 1E).

### RXFP1 deficiency resulted in increased inflammation of AVF lesions

Immunohistochemical analysis of sections obtained from the venous outflow tract showed a 6-fold increase in the number of CD45<sup>+</sup> leukocytes in lesions of  $Rxfp1^{-/-}$  mice when compared with WT mice ( $P = 0.02$ ) (Fig. 2A). As shown in Fig. 2B, C, further characterization of the leukocyte subpopulations revealed a 4-fold increase in the number of proinflammatory Mac3<sup>+</sup>/CCR2<sup>+</sup> macrophages ( $P = 0.02$ ) and a 43% increase in the Mac3<sup>+</sup>/CD206<sup>+</sup> anti-inflammatory macrophages in the lesions from  $Rxfp1^{-/-}$  mice ( $P = 0.04$ ). The number of GR1<sup>+</sup> neutrophils was 3-fold higher in  $Rxfp1^{-/-}$  mice than in WT mice ( $P = 0.05$ ) (Fig. 2D). The number of CD3<sup>+</sup> T-lymphocytes in the venous outflow tract was not affected by RXFP1 deficiency (Supplemental Fig. 3). At the level of cytokine production within the lesions, MCP1 expression was 2-fold greater in  $Rxfp1^{-/-}$  mice than in WT mice ( $P = 0.01$ ) (Fig. 3).

*In vitro*, activated macrophages that were differentiated from monocytes derived from  $Rxfp1^{-/-}$  mice produced a similar amount of cytokines as WT mice did; ELISA analysis demonstrated comparable expression of MCP1, IL12, and IL10 proteins (data not shown).

### Phenotypic switch of arterial and venous VSMCs upon RXFP1 deletion

The impact of RXFP1 deficiency on the VSMC phenotype was studied *in vitro* using primary arterial and venous VSMCs isolated from the aorta and caval vein, respectively, of  $Rxfp1^{-/-}$  or WT mice. Phenotypic difference of arterial and venous VSMCs was confirmed by mRNA levels of ephrin B2, an established embryological marker of arterial origin (35). EphrinB2 was increased in arterial VSMCs from both WT and  $Rxfp1^{-/-}$  mice following 2 wk of culture, but not in venous VSMCs (Fig. 4A). Further characterization of these VSMCs confirmed that the cells



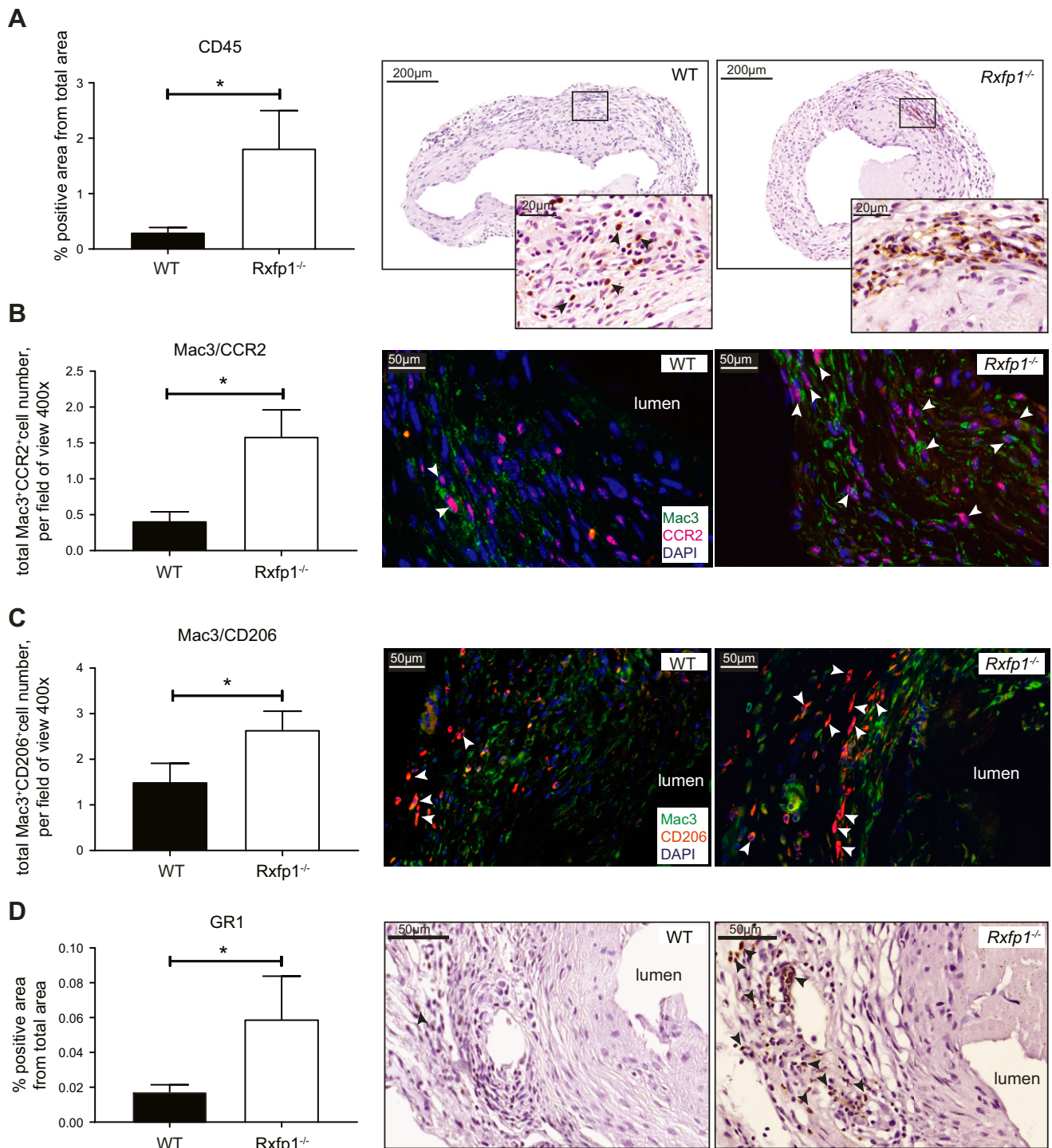


**Figure 2.** Effects of RXFP1 deficiency on inflammatory status *in vivo*. Quantification and immunohistochemical staining of CD45<sup>+</sup> leukocytes (black arrows) (A), MAC3<sup>+</sup>/CCR2<sup>+</sup> macrophages (B), MAC3<sup>+</sup>/CD206<sup>+</sup> macrophages (white arrows) (C), and GR1<sup>+</sup> neutrophils (black arrows) (D) in the AVF lesions 14 d after surgery. All cell populations were higher in the lesions from *Rxfp1*<sup>-/-</sup> mice compared with those in the WT. \**P* < 0.05 (*n* = 10/group).

maintained a highly differentiated state, as evidenced by the maintenance of myosin heavy chain, calponin, and caldesmon expression at 2 wk of culture (Fig. 4B).

Because vascular injury and remodeling trigger the phenotypic switch of VSMCs from a contractile to a synthetic state, mRNA expression levels of several genes associated with this switch were measured (36, 37). Arterial VSMCs from *Rxfp1*<sup>-/-</sup> mice expressed markedly higher

levels of the synthetic VSMC markers type I collagen (38) and fibronectin (39) than did VSMCs derived from WT mice [5-fold (*P* = 0.03) and 10-fold (*P* = 0.04), respectively]. Similarly, the mRNA expression levels of both type I collagen and fibronectin were higher in venous VSMCs harvested from *Rxfp1*<sup>-/-</sup> mice [3-fold (*P* = 0.05) and 4-fold (*P* = 0.04), respectively]. Furthermore, genes linked with cellular proliferation, such as TGF-β1 (40) and platelet-derived

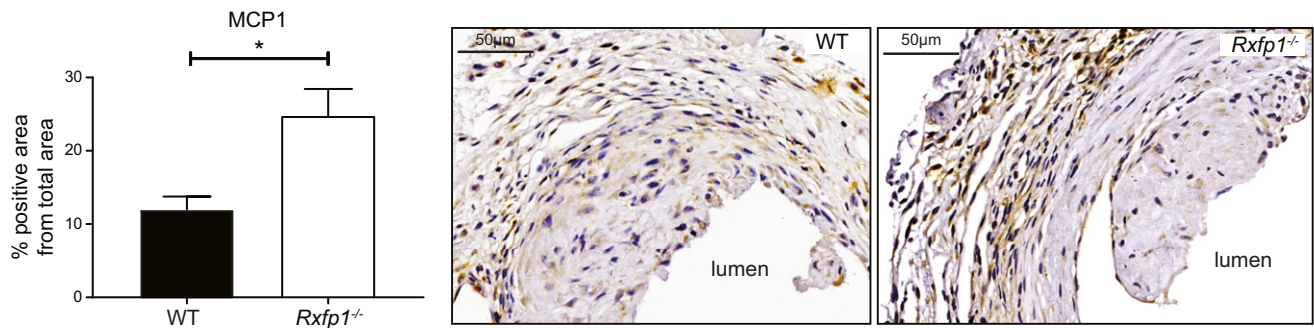


**Figure 3.** Accumulation of MCP1 in the AVF lesions from *Rxfp1*<sup>-/-</sup> and WT mice 14 d after surgery. RXFP1 deficiency resulted in greater MCP1 expression (brown DAB signal) than that found in WT mice. \**P* < 0.05 (*n* = 10/group).

growth factor (41), displayed on average 3-fold higher expression levels in both arterial and venous VSMCs isolated from *Rxfp1*<sup>-/-</sup> mice than did WT mice (Fig. 4C).

To further examine whether RLN deficiency impacts VSMC function, we performed cellular migration assays. These studies revealed that arterial VSMCs derived from

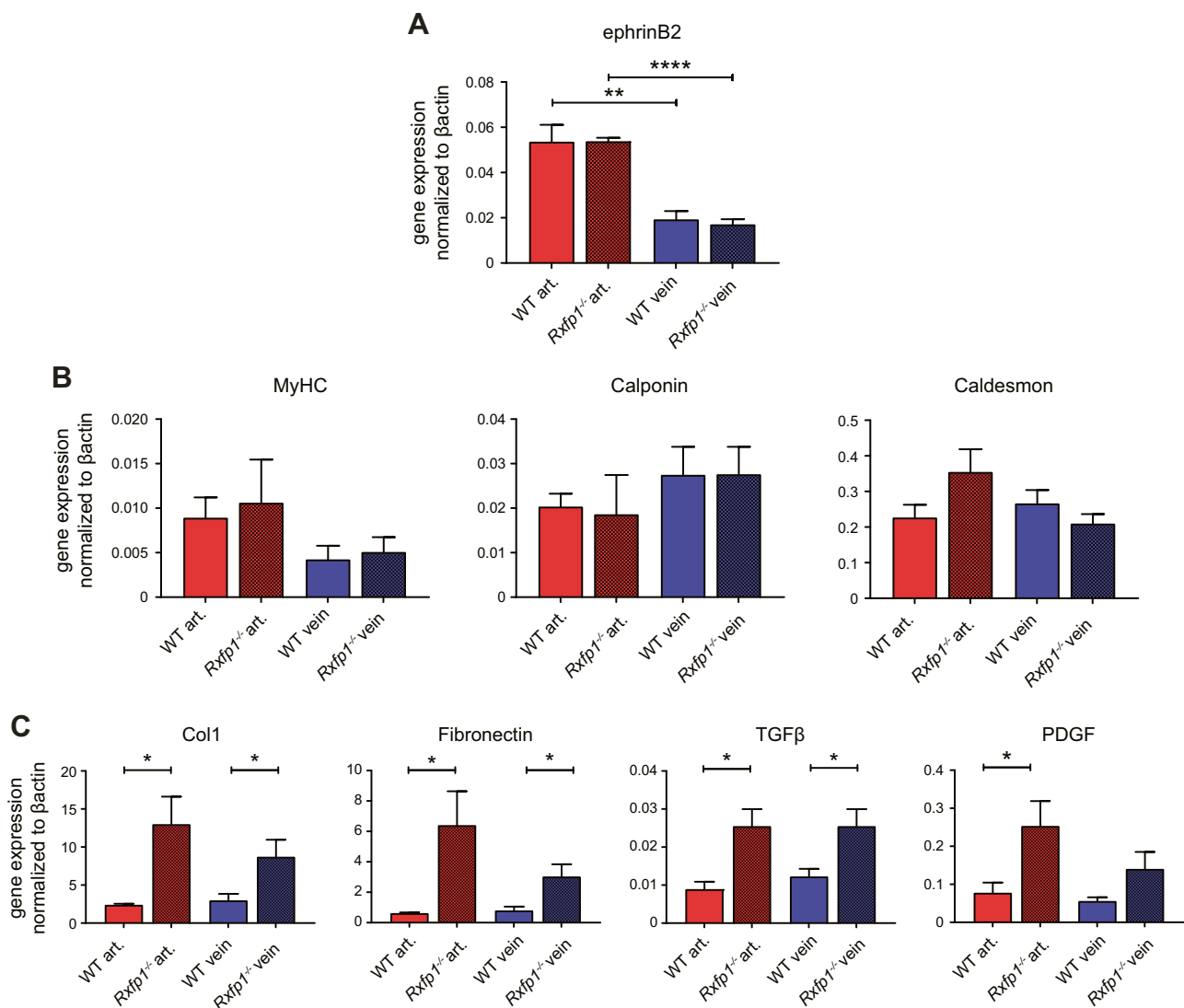


**Figure 4.** *In vitro* phenotypic difference between primary arterial and venous VSMCs isolated from *Rxfp1*<sup>-/-</sup> and WT mice. A) Stable increase in ephrinB2 gene expression was detected in arterial VSMCs isolated from WT and *Rxfp1*<sup>-/-</sup> mice. B) Both arterial and venous VSMCs isolated from *Rxfp1*<sup>-/-</sup> and WT displayed characteristics of mature VSMCs as confirmed by a stable expression of myosin heavy chain, calponin, and caldesmon genes. C) RXFP1 deficiency resulted in a switch of arterial and venous VSMCs to a synthetic phenotype as confirmed by increased collagen I (Col1), fibronectine, TGF-β, and platelet-derived growth factor mRNA expression levels. VSMCs were maintained in culture for 14 d. \**P* < 0.05, \*\**P* < 0.005, \*\*\*\**P* < 0.0001 (*n* = 4).

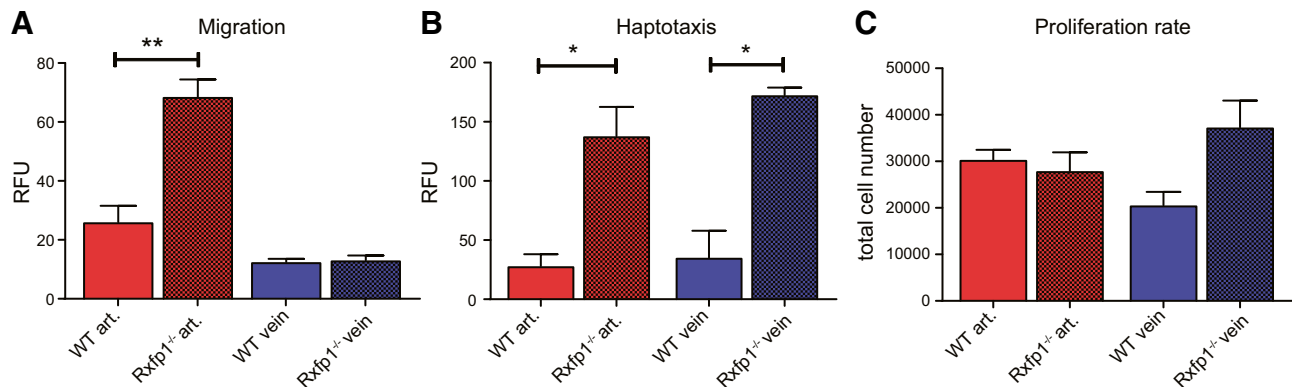


**Figure 5.** Effect of RXFP1 deficiency on VSMCs function *in vitro*. *A, B*) Increase in migration (*A*) of VSMCs isolated from *Rxfp1*<sup>-/-</sup> mice was restricted to arterial cells only, whereas cellular haptotaxis or migration through the layer of collagen (*B*) was increased on both arterial and venous cells isolated from *Rxfp1*<sup>-/-</sup> mice. *C*) Proliferation rate did not differ between *Rxfp1*<sup>-/-</sup> and WT mice. Cells were cultured for 14 d. Migration, haptotaxis, and proliferation were measured over a 16 h time period. \**P* < 0.05, \*\**P* < 0.005 (*n* = 4).

*Rxfp1*<sup>-/-</sup> display a significantly higher migratory capacity relative to VSMCs derived from WT mice, whereas migration of venous VSMCs was unaltered (Fig. 5A). To mimic VSMC migration within the ECM of a blood vessel, a haptotaxis assay was performed to evaluate cellular migration in a matrix of type I collagen. As shown in Fig. 5B, we observed enhanced migration of arterial and venous VSMCs derived from *Rxfp1*<sup>-/-</sup> mice when compared with WT [5-fold (*P* = 0.05) and 5-fold (*P* = 0.03), respectively]. In contrast, cellular proliferation was not affected by RLN deficiency in either arterial or venous VSMCs (Fig. 5C). *In vivo*, the number of proliferating cells in the venous outflow tract of AVF did not differ significantly between groups (Supplemental Fig. 4).

### Elastin metabolism in AVF lesions of RXFP1-deficient mice

Having observed higher elastin content in the venous outflow tract of AVF in *Rxfp1*<sup>-/-</sup> mice, we next assessed elastase activity in sections obtained from the venous outflow tract of the AVF. We employed the EnzChek assay, which measures fluorescence of the substrate (bovine elastin) digested by elastase. Elastase activity was significantly lower in AVFs from *Rxfp1*<sup>-/-</sup> mice than in AVFs derived from WT mice (*P* = 0.0001) (Fig. 6).

*Ex vivo*, elastin synthesis in cultured arterial and venous VSMCs isolated from *Rxfp1*<sup>-/-</sup> or WT mice did not differ because mRNA expression levels of tropoelastin were similar between the groups (Supplemental Fig. 5).

### In humans RXFP1 expression increases during AVF maturation

To explore the relevance of our observations for dialysis patients, we examined 3 specimens of cephalic vein before AVF surgery and during surgical revisions of AVF. Immunohistochemical analysis revealed increased RLN2 and RXFP1 expression in the cephalic outflow tract of AVF, when compared with segments of cephalic veins from patients with end-stage renal failure during primary

AVF surgery (Fig. 7A). Cells that expressed RLN2 and RXFP1 were enriched in the intimal region of the outflow tract and were found to coexpress  $\alpha$ SMA (Fig. 7B). These results strongly suggest that RLN2 and RXFP1 expression is elevated in the venous outflow tract of human AVFs, which underscores the relevance of these proteins in the process of AVF maturation in humans.

## DISCUSSION

Here, we show that although RXFP1 deficiency substantially impairs OR in a murine model of AVF, no effect on IH is observed. Our findings pinpoint an increase in elastin content in the venous outflow tract in RXFP1-deficient mice linked with attenuated elastase activity as a

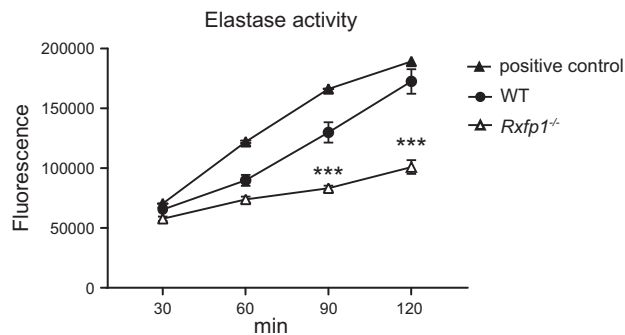


**Figure 6.** Kinetics of the elastase activity in the lesions of *Rxfp1*<sup>-/-</sup> and WT mice 14 d after surgery. AVF tissue lysates from WT and *Rxfp1*<sup>-/-</sup> mice were incubated with DQ elastin at a final concentration of 25  $\mu$ g/ml for the indicated time periods. Elastase activity in AVFs from *Rxfp1*<sup>-/-</sup> mice (white triangles) was significantly lower after 90- and 120-min incubation time than that found in AVFs derived from WT mice (black circles). Fluorescence was measured in a fluorescence multiwell plate reader set for excitation at 485  $\pm$  10 nm and emission detection at 530  $\pm$  15 nm. Porcine pancreatic elastase (0.2 U/ml) was used as positive control (black triangles). Background fluorescence, determined for a no-enzyme control reaction, has been subtracted from each value. \*\*\**P* = 0.0002 (*n* = 10/group).



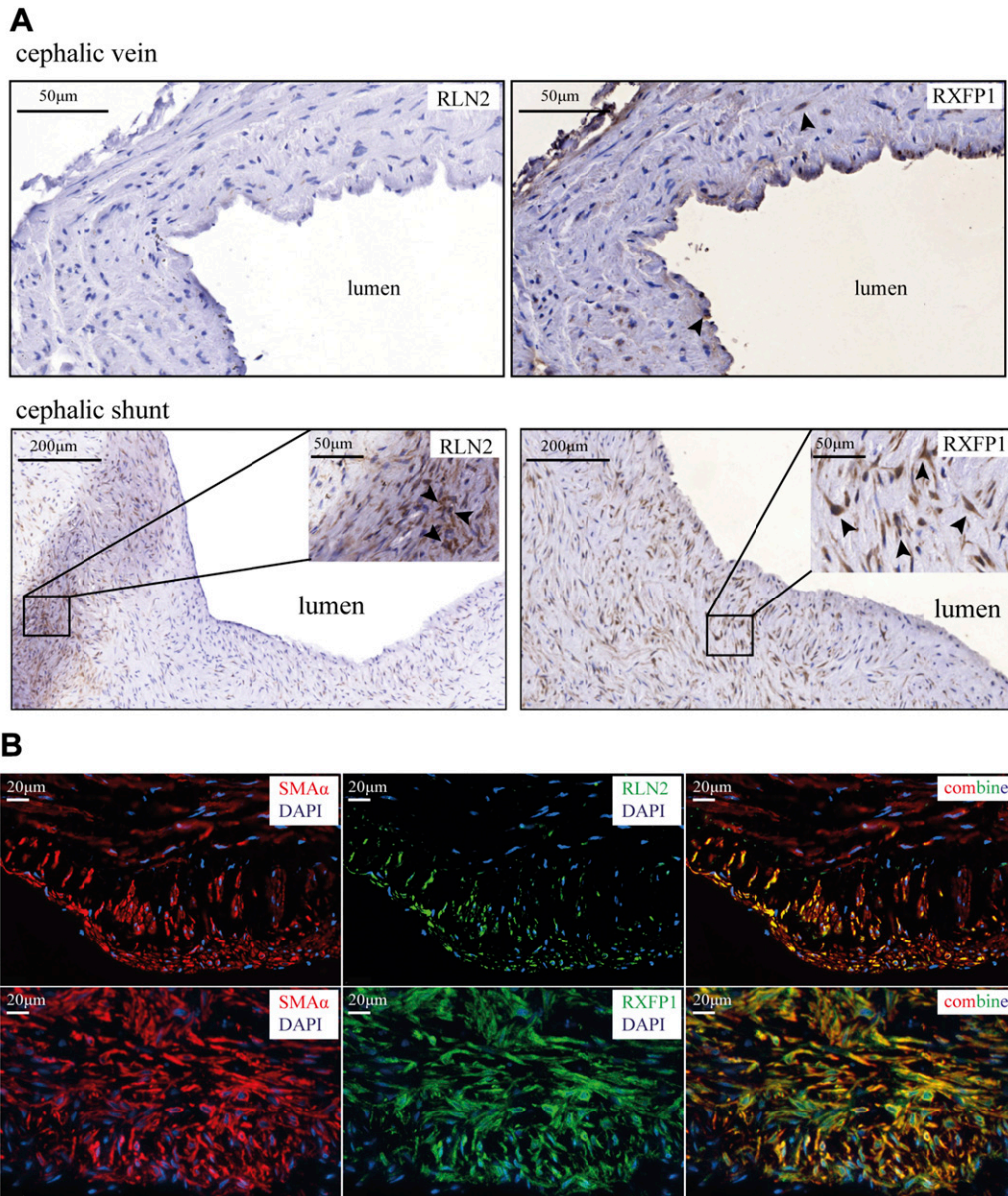


**Figure 7.** Expression of RLN2 and RXFP1 proteins by  $\alpha$ SMA<sup>+</sup> cells in dialysis patients. *A*) Representative images of RLN2 and RXFP1 proteins (black arrows) in human cephalic veins prior to AVF surgery and cephalic venous outflow tract from AVF. *B*) Cells positive for RLN2 and RXFP1 (green) were mainly located in the intimal region and were coexpressing  $\alpha$ SMA (red);  $n = 3$ .

potential cause for this phenotype. As such, impaired elastin degradation in combination with enhanced vascular inflammation after AVF surgery likely triggers adverse vascular response in humans following the placement of an AVF.

### Impaired elastin degradation and vascular remodeling in RXFP1-deficient mice

Expansion of the venous lumen and an initial vasodilatory response are prerequisites for successful AVF maturation and patency. In particular, the process of OR plays a pivotal role in this process. Although past research has focused mainly on the development of strategies to reduce IH, the current view on AVF maturation underscores the link between impaired OR and AVF failure (42, 43). To promote

OR, matrix metalloproteinase expression must be augmented to degrade and restructure the vascular matrix (44), which is largely composed of elastic fibers. Interestingly, periaortitis application of recombinant elastase has been shown to stimulate OR in a rabbit model of AVF (45). Interestingly, this concept of pharmacological elastin degradation to promote AVF maturation is now being evaluated in phase III clinical trials (46).

Enhanced expression of RLN is critical for ECM remodeling in the cervix and myometrium during pregnancy (47, 48). Administration of recombinant RLN increases the activity of elastase in human myometrial cells (26). Our discovery that RXFP1 deficiency significantly reduced elastase activity, resulting in elastic fiber accumulation in AVF lesions, suggests that RXFP1 is an important regulator of elastin degradation during AVF maturation. Furthermore, it supports the concept that



- Outcomes of arteriovenous fistula creation after the Fistula First Initiative. *Clin. J. Am. Soc. Nephrol.* **6**, 1996–2002
2. Al-Jaishi, A. A., Oliver, M. J., Thomas, S. M., Lok, C. E., Zhang, J. C., Garg, A. X., Kosa, S. D., Quinn, R. R., and Moist, L. M. (2014) Patency rates of the arteriovenous fistula for hemodialysis: a systematic review and meta-analysis. *Am. J. Kidney Dis.* **63**, 464–478
  3. Rothuizen, T. C., Wong, C., Quax, P. H., van Zonneveld, A. J., Rabelink, T. J., and Rotmans, J. I. (2013) Arteriovenous access failure: more than just intimal hyperplasia? *Nephrol. Dial. Transplant.* **28**, 1085–1092
  4. Wong, C., Bezhaeva, T., Rothuizen, T. C., Metselaar, J. M., de Vries, M. R., Verbeek, F. P., Vahrmeijer, A. L., Wezel, A., van Zonneveld, A. J., Rabelink, T. J., Quax, P. H., and Rotmans, J. I. (2016) Liposomal prednisolone inhibits vascular inflammation and enhances venous outward remodeling in a murine arteriovenous fistula model. *Sci. Rep.* **6**, 30439
  5. Wong, C.-Y., de Vries, M. R., Wang, Y., van der Vorst, J. R., Vahrmeijer, A. L., van Zonneveld, A. J., Roy-Chaudhury, P., Rabelink, T. J., Quax, P. H. A., and Rotmans, J. I. (2014) Vascular remodeling and intimal hyperplasia in a novel murine model of arteriovenous fistula failure. *J. Vasc. Surg.* **59**, 192–201.e1
  6. Bezhaeva, T., Wong, C., de Vries, M. R., van der Veer, E. P., van Alem, C. M. A., Que, I., Lalai, R. A., van Zonneveld, A. J., Rotmans, J. I., and Quax, P. H. A. (2017) Deficiency of TLR4 homologue RP105 aggravates outward remodeling in a murine model of arteriovenous fistula failure. *Sci. Rep.* **7**, 10269
  7. Krishnamoorthy, M. K., Banerjee, R. K., Wang, Y., Zhang, J., Sinha Roy, A., Khoury, S. F., Arend, L. J., Rudich, S., and Roy-Chaudhury, P. (2008) Hemodynamic wall shear stress profiles influence the magnitude and pattern of stenosis in a pig AV fistula. *Kidney Int.* **74**, 1410–1419
  8. Liang, M., Wang, Y., Liang, A., Mitch, W. E., Roy-Chaudhury, P., Han, G., and Cheng, J. (2015) Migration of smooth muscle cells from the arterial anastomosis of arteriovenous fistulas requires Notch activation to form neointima. *Kidney Int.* **88**, 490–502
  9. Roy-Chaudhury, P., Wang, Y., Krishnamoorthy, M., Zhang, J., Banerjee, R., Munda, R., Heffelfinger, S., and Arend, L. (2009) Cellular phenotypes in human stenotic lesions from haemodialysis vascular access. *Nephrol. Dial. Transplant.* **24**, 2786–2791
  10. Roy-Chaudhury, P., Khan, R., Campos, B., Wang, Y., Kurian, M., Lee, T., Arend, L., and Munda, R. (2014) Pathogenetic role for early focal macrophage infiltration in a pig model of arteriovenous fistula (AVF) stenosis. *J. Vasc. Access* **15**, 25–28
  11. Zhao, J., Jourd'heuil, F. L., Xue, M., Conti, D., Lopez-Soler, R. I., Ginnan, R., Asif, A., Singer, H. A., Jourd'heuil, D., and Long, X. (2017) Dual function for mature vascular smooth muscle cells during arteriovenous fistula remodeling. *J. Am. Heart Assoc.* **6**, e004891
  12. Conrad, K. P., Debrah, D. O., Novak, J., Danielson, L. A., and Shroff, S. G. (2004) Relaxin modifies systemic arterial resistance and compliance in conscious, nonpregnant rats. *Endocrinology* **145**, 3289–3296
  13. Feng, S., Bogatcheva, N. V., Kamat, A. A., Truong, A., and Agoulnik, A. I. (2006) Endocrine effects of relaxin overexpression in mice. *Endocrinology* **147**, 407–414
  14. Cernaro, V., Lacquaniti, A., Lupica, R., Buemi, A., Trimboli, D., Giorgianni, G., Bolignano, D., and Buemi, M. (2014) Relaxin: new pathophysiological aspects and pharmacological perspectives for an old protein. *Med. Res. Rev.* **34**, 77–105
  15. Jeyabalan, A., Shroff, S. G., Novak, J., and Conrad, K. P. (2007) The vascular actions of relaxin. *Adv. Exp. Med. Biol.* **612**, 65–87
  16. Sherwood, O. D. (2004) Relaxin's physiological roles and other diverse actions. *Endocr. Rev.* **25**, 205–234
  17. Debrah, D. O., Conrad, K. P., Jeyabalan, A., Danielson, L. A., and Shroff, S. G. (2005) Relaxin increases cardiac output and reduces systemic arterial load in hypertensive rats. *Hypertension* **46**, 745–750
  18. Conrad, K. P., and Shroff, S. G. (2011) Effects of relaxin on arterial dilation, remodeling, and mechanical properties. *Curr. Hypertens. Rep.* **13**, 409–420
  19. Debrah, D. O., Debrah, J. E., Haney, J. L., McGuane, J. T., Sacks, M. S., Conrad, K. P., and Shroff, S. G. (2011) Relaxin regulates vascular wall remodeling and passive mechanical properties in mice. *J. Appl. Physiol.* **111**, 260–271
  20. Chan, S. L., and Cipolla, M. J. (2011) Relaxin causes selective outward remodeling of brain parenchymal arterioles via activation of peroxisome proliferator-activated receptor- $\gamma$ . *FASEB J.* **25**, 3229–3239
  21. Samuel, C. S., Lekgabe, E. D., and Mookerjee, I. (2007) The effects of relaxin on extracellular matrix remodeling in health and fibrotic disease. *Adv. Exp. Med. Biol.* **612**, 88–103
  22. Samuel, C. S., and Hewitson, T. D. (2009) Relaxin and the progression of kidney disease. *Curr. Opin. Nephrol. Hypertens.* **18**, 9–14
  23. Chow, B. S., Kocan, M., Bosnyak, S., Sarwar, M., Wigg, B., Jones, E. S., Widdop, R. E., Summers, R. J., Bathgate, R. A., Hewitson, T. D., and Samuel, C. S. (2014) Relaxin requires the angiotensin II type 2 receptor to abrogate renal interstitial fibrosis. *Kidney Int.* **86**, 75–85
  24. Zhou, X., Chen, X., Cai, J. J., Chen, L. Z., Gong, Y. S., Wang, L. X., Gao, Z., Zhang, H. Q., Huang, W. J., and Zhou, H. (2015) Relaxin inhibits cardiac fibrosis and endothelial–mesenchymal transition via the Notch pathway. *Drug Des. Devel. Ther.* **9**, 4599–4611
  25. Bennett, R. G., Heimann, D. G., Singh, S., Simpson, R. L., and Tuma, D. J. (2014) Relaxin decreases the severity of established hepatic fibrosis in mice. *Liver Int.* **34**, 416–426
  26. Chen, B., Wen, Y., Yu, X. Y., and Polan, M. L. (2009) Relaxin increases elastase activity and protease inhibitors in smooth muscle cells from the myometrium compared with cells from leiomyomas. *Fertil. Steril.* **91** (4 Suppl.), 1351–1354
  27. Brecht, A., Bartsch, C., Baumann, G., Stangl, K., and Dschietzig, T. (2011) Relaxin inhibits early steps in vascular inflammation. *Regul. Pept.* **166**, 76–82
  28. Novak, J., Parry, L. J., Matthews, J. E., Kerchner, L. J., Indovina, K., Hanley-Yanez, K., Doty, K. D., Debrah, D. O., Shroff, S. G., and Conrad, K. P. (2006) Evidence for local relaxin ligand-receptor expression and function in arteries. *FASEB J.* **20**, 2352–2362
  29. Jelincic, M., Leo, C. H., Post Uiterweer, E. D., Sandow, S. L., Gooi, J. H., Wlodek, M. E., Conrad, K. P., Parkington, H., Tare, M., and Parry, L. J. (2014) Localization of relaxin receptors in arteries and veins, and region-specific increases in compliance and bradykinin-mediated relaxation after in vivo sere relaxin treatment. *FASEB J.* **28**, 275–287
  30. Bathgate, R. A., Halls, M. L., van der Westhuizen, E. T., Callander, G. E., Kocan, M., and Summers, R. J. (2013) Relaxin family peptides and their receptors. *Physiol. Rev.* **93**, 405–480
  31. Horton, J. S., Yamamoto, S. Y., and Bryant-Greenwood, G. D. (2011) Relaxin modulates proinflammatory cytokine secretion from human decidual macrophages. *Biol. Reprod.* **85**, 788–797
  32. Leo, C. H., Jelincic, M., Ng, H. H., Marshall, S. A., Novak, J., Tare, M., Conrad, K. P., and Parry, L. J. (2017) Vascular actions of relaxin: nitric oxide and beyond. *Br. J. Pharmacol.* **174**, 1002–1014
  33. Kamat, A. A., Feng, S., Bogatcheva, N. V., Truong, A., Bishop, C. E., and Agoulnik, A. I. (2004) Genetic targeting of relaxin and insulin-like factor 3 receptors in mice. *Endocrinology* **145**, 4712–4720
  34. Wong, C. Y., de Vries, M. R., Wang, Y., van der Vorst, J. R., Vahrmeijer, A. L., van Zonneveld, A. J., Hamming, J. F., Roy-Chaudhury, P., Rabelink, T. J., Quax, P. H., and Rotmans, J. I. (2016) A novel murine model of arteriovenous fistula failure: the surgical procedure in detail. *J. Vis. Exp.* **108**, e53294
  35. Shin, D., Garcia-Cardena, G., Hayashi, S., Gerety, S., Asahara, T., Stavrikis, G., Isner, J., Folkman, J., Gimbrone, M. A., Jr., and Anderson, D. J. (2001) Expression of ephrinB2 identifies a stable genetic difference between arterial and venous vascular smooth muscle as well as endothelial cells, and marks subsets of microvessels at sites of adult neovascularization. *Dev. Biol.* **230**, 139–150
  36. Owens, G. K., Kumar, M. S., and Wamhoff, B. R. (2004) Molecular regulation of vascular smooth muscle cell differentiation in development and disease. *Physiol. Rev.* **84**, 767–801
  37. Lacolley, P., Regnault, V., Nicoletti, A., Li, Z., and Michel, J. B. (2012) The vascular smooth muscle cell in arterial pathology: a cell that can take on multiple roles. *Cardiovasc. Res.* **95**, 194–204
  38. Ichii, T., Koyama, H., Tanaka, S., Kim, S., Shioi, A., Okuno, Y., Raines, E. W., Iwao, H., Otani, S., and Nishizawa, Y. (2001) Fibrillar collagen specifically regulates human vascular smooth muscle cell genes involved in cellular responses and the pericellular matrix environment. *Circ. Res.* **88**, 460–467
  39. Thyberg, J., and Hultgårdh-Nilsson, A. (1994) Fibronectin and the basement membrane components laminin and collagen type IV influence the phenotypic properties of subcultured rat aortic smooth muscle cells differently. *Cell Tissue Res.* **276**, 263–271
  40. Hocevar, B. A., and Howe, P. H. (2000) Analysis of TGF $\beta$ -mediated synthesis of extracellular matrix components. *Methods Mol. Biol.* **142**, 55–65
  41. Kingsley, K., Huff, J. L., Rust, W. L., Carroll, K., Martinez, A. M., Fitchmun, M., and Plopper, G. E. (2002) ERK1/2 mediates PDGF-BB stimulated vascular smooth muscle cell proliferation and migration on laminin-5. *Biochem. Biophys. Res. Commun.* **293**, 1000–1006

42. Lee, T., and Misra, S. (2016) New insights into dialysis vascular access: molecular targets in arteriovenous fistula and arteriovenous graft failure and their potential to improve vascular access outcomes. *Clin. J. Am. Soc. Nephrol.* **11**, 1504–1512
43. Guzman, R. J., Abe, K., and Zarins, C. K. (1997) Flow-induced arterial enlargement is inhibited by suppression of nitric oxide synthase activity *in vivo*. *Surgery* **122**, 273–280
44. Chan, C. Y., Chen, Y. S., Ma, M. C., and Chen, C. F. (2007) Remodeling of experimental arteriovenous fistula with increased matrix metalloproteinase expression in rats. *J. Vasc. Surg.* **45**, 804–811
45. Burke, S. K., Franano, F. N., LaRochelle, A., and Mendenhall, H. V. (2008) Local application of recombinant human type I pancreatic elastase (PRT-201) to an arteriovenous fistula (AVF) increases AVF blood flow in a rabbit model. *J. Am. Soc. Nephrol.* **19**, 252–253
46. Peden, E. K., O'Connor, T. P., Browne, B. J., Dixon, B. S., Schanzer, A. S., Jensik, S. C., Sam, A. D. II, and Burke, S. K. (2017) Arteriovenous fistula patency in the 3 years following vonapanitase and placebo treatment. *J. Vasc. Surg.* **65**, 1113–1120
47. Finlay, G. A., O'Donnell, M. D., O'Connor, C. M., Hayes, J. P., and FitzGerald, M. X. (1996) Elastin and collagen remodeling in emphysema. A scanning electron microscopy study. *Am. J. Pathol.* **149**, 1405–1415
48. Chen, B., Wen, Y., Yu, X., and Polan, M. L. (2005) Elastin metabolism in pelvic tissues: is it modulated by reproductive hormones? *Am. J. Obstet. Gynecol.* **192**, 1605–1613
49. Kang, L., Grande, J. P., Hillestad, M. L., Croatt, A. J., Barry, M. A., Katusic, Z. S., and Nath, K. A. (2016) A new model of an arteriovenous fistula in chronic kidney disease in the mouse: beneficial effects of upregulated heme oxygenase-1. *Am. J. Physiol. Renal Physiol.* **310**, F466–F476
50. Kang, L., Grande, J. P., Farrugia, G., Croatt, A. J., Katusic, Z. S., and Nath, K. A. (2013) Functioning of an arteriovenous fistula requires heme oxygenase-2. *Am. J. Physiol. Renal Physiol.* **305**, F545–F552
51. Juncos, J. P., Grande, J. P., Kang, L., Ackerman, A. W., Croatt, A. J., Katusic, Z. S., and Nath, K. A. (2011) MCP-1 contributes to arteriovenous fistula failure. *J. Am. Soc. Nephrol.* **22**, 43–48
52. Wolf, K., Te Lindert, M., Krause, M., Alexander, S., Te Riet, J., Willis, A. L., Hoffman, R. M., Figdor, C. G., Weiss, S. J., and Friedl, P. (2013) Physical limits of cell migration: control by ECM space and nuclear deformation and tuning by proteolysis and traction force. *J. Cell Biol.* **201**, 1069–1084
53. Teerlink, J. R., Cotter, G., Davison, B. A., Felker, G. M., Filippatos, G., Greenberg, B. H., Ponikowski, P., Unemori, E., Voors, A. A., Adams, K. F., Jr., Dorobantu, M. I., Grinfeld, L. R., Jondeau, G., Marmor, A., Masip, J., Pang, P. S., Werdan, K., Teichman, S. L., Trapani, A., Bush, C. A., Saini, R., Schumacher, C., Severin, T. M., and Metra, M.; RELAXin in Acute Heart Failure (RELAX-AHF) Investigators. (2013) Serelaxin, recombinant human relaxin-2, for treatment of acute heart failure (RELAX-AHF): a randomised, placebo-controlled trial. *Lancet* **381**, 29–39
54. Xiao, J., Huang, Z., Chen, C. Z., Agoulnik, I. U., Southall, N., Hu, X., Jones, R. E., Ferrer, M., Zheng, W., Agoulnik, A. I., and Marugan, J. J. (2013) Identification and optimization of small-molecule agonists of the human relaxin hormone receptor RXFP1. *Nat. Commun.* **4**, 1953

Received for publication March 7, 2018.  
Accepted for publication May 14, 2018.